Dynamic Source Localization via Finite-Element Underwater Acoustic Field Estimation

Graziano A. Manduzio*, Nicola Forti†, Roberto Sabatini†, Paolo Braca†, Giorgio Battistelli*, and Luigi Chisci*
*Università degli Studi di Firenze, Firenze, Italy, Email: *{grazianoalfredo.manduzio,giorgio.battistelli,luigi.chisci}@unifi.it
†NATO STO Centre for Maritime Research and Experimentation, La Spezia, Italy, Email: †{name.surname}@cmre.nato.int

***Abstract*—In this paper we address the problem of dynamic source localization in spatially distributed systems governed by Partial Differential Equations (PDEs) which aims to detect and localize a mobile source from a passive array of acoustic sensors. We consider an underwater environment where the space-time dynamics of the source-induced field is modeled by a finite-element (FE) approximation of the full acoustic wave PDE. Based on recent advancements in large-scale state estimation of PDE systems, we present a novel Multiple Model (MM) filtering approach to underwater dynamic source localization. The proposed framework sequentially estimates the acoustic field and the source location by running in parallel a bank of FE-based field estimators, each conditioned to the source being placed in a given element of the FE mesh. We adopt the Ensemble Kalman Filter (EnKF) implementation for computationally efficient estimation of the large-scale acoustic field. The effectiveness of the proposed Finite-Element Multiple Model Ensemble Kalman Filter (FE-MM-EnKF) is demonstrated via simulation experiments in the underwater acoustic environment.**

I. Introduction

Due to the special characteristics and complexity of the underwater environment, localization and tracking of a moving acoustic source using a passive array system of acoustic sensors is a challenging task, especially in low signal-to-noise ratio (SNR) scenarios, where the source can be difficult to detect [1]. Conventional signal processing methods based on matched-field processing (MFP) [2] and bearing-only tracking (BOT) [3]–[5] may not be able to detect such low-observable targets. Source localization using common MFP methods is effective when the source is stationary and the propagation model is completely known. However, it can be highly degraded or precluded in the case of noisy or uncertain sources and environmental parameters [6]. Source motion is an additional factor of performance degradation, for which ad-hoc extensions of MFP [7]–[9] need to be taken into account when dealing with dynamic sources. On the other hand, classical BOT methods can only exploit thresholded bearing measurements. In low SNR environments the acoustic signals are distorted by ambient noise and are more likely to be undetected using conventional BOT methods since the information contained in the measurements may be irreversibly discarded after the thresholding process [10]–[12].

In order to provide reliable and faster detection/localization of a moving source, the proposed method explicitly takes into account the space-time acoustic field dynamics modeled by an FE approximation of the full acoustic wave PDE. This allows the original infinite-dimensional initial-boundary value problem to be transformed into a finite-dimensional discrete-time linear system, with state vector consisting of the field values in the vertices of the FE mesh and input matrix depending on the source location. Based on recent advancements in numerical simulation [13] and large-scale dynamic state estimation of PDE systems [14], [15], we developed a novel Finite-Element Multiple Model Ensemble Kalman Filter (FE-MM-EnKF) for underwater dynamic source localization. The proposed framework sequentially estimates the acoustic field and the source location by running in parallel a bank of FE-based field estimators implemented in the EnKF [16] fashion, each conditioned to the source being placed in a given element of the FE mesh, plus a null hypothesis representing the absence of the source.

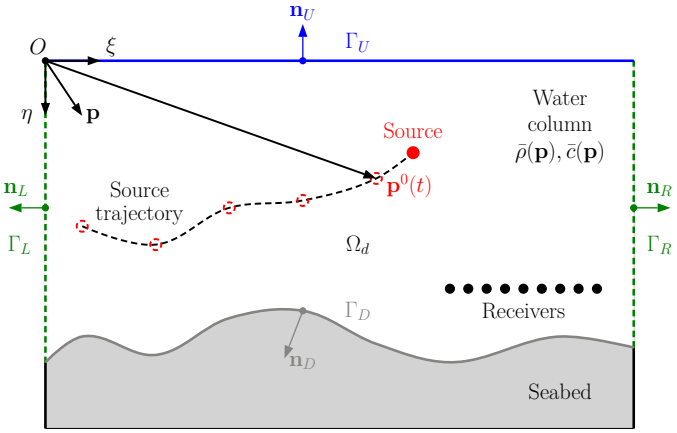

Fig. 1: Example of dynamic source localization in an underwater acoustic environment.

The proposed method can enhance the detection, localization, and tracking performance of low-observable underwater targets by exploiting FE-based acoustic field estimation directly from raw acoustic pressure measurements. Further advantages of the proposed framework with respect to conventional BOT methods include the fact that i) it does not require an intermediate step of bearing estimation; ii) it leads to a (large-scale) linear instead of nonlinear estimation problem; iii) it incorporates an FE model of underwater acoustic propagation for advanced numerical simulation in the time domain.

This work was funded by the NATO Allied Command Transformation (ACT) under the project Data Knowledge Operational Effectiveness.

II. Problem formulation

Consider the two-dimensional infinite oceanic waveguide Ω depicted in Fig. 1, bounded from above by a flat free surface Γ_U and from below by a possibly irregular seabed Γ_D. Define a Cartesian coordinate system $O\xi\eta$, with the origin O on Γ_U and the vertical axis η oriented toward the seafloor, and denote $\mathbf{p} \in \Omega$ the position vector and $t \in \mathbb{R}^+$ the time variable. Let $\bar{c}(\mathbf{p})$ and $\bar{\rho}(\mathbf{p})$ be the space-dependent ambient speed of sound and water density, respectively. Suppose that a perturbation of pressure $x(\mathbf{p}, t)$ is induced in the water column by a moving point source $f(\mathbf{p}, t)$. The goal is to detect the presence of the sound emitter and jointly estimate its location as well as the source-induced acoustic field $x(\mathbf{p}, t)$, given a certain number of pointwise-in-space-and-in-time measurements. To this end, the propagation of the perturbation of pressure $x(\mathbf{p}, t)$ is assumed governed by the generalized wave equation [1]

$$\frac{1}{\bar{\rho}\bar{c}^2}\frac{\partial^2 x}{\partial t^2} - \nabla \cdot \left(\frac{1}{\bar{\rho}}\nabla x\right) - \frac{f}{\bar{\rho}} = 0, \tag{1a}$$

with initial conditions

$$x(\mathbf{p}, t=0) = 0, \quad \frac{\partial x}{\partial t}(\mathbf{p}, t=0) = 0, \quad \forall \mathbf{p} \in \Omega, \tag{1b}$$

and boundary constraints

$$\begin{aligned} x &= 0 \qquad\qquad \forall t \in \mathbb{R}^+, \forall \mathbf{p} \in \Gamma_U, \\ \nabla x \cdot \mathbf{n}_D &= 0 \quad \forall t \in \mathbb{R}^+, \forall \mathbf{p} \in \Gamma_D. \end{aligned} \tag{1c}$$

The forcing term is nil in the absence of sources and modeled as $f(\mathbf{p}, t) = s(t)\,\delta\left(\mathbf{p} - \mathbf{p}^0(t)\right)$ otherwise, where $s(t)$ is a temporal envelope, $\mathbf{p}^0(t)$ is the instantaneous position of the source, and δ is the Dirac delta function.

III. Finite-element discretization and time integration

Problem (1) is solved numerically through the FE method. To this end, the infinite domain Ω is first truncated along the horizontal axis, as illustrated in Fig. 1. The resulting computational domain Ω_d is delimited by the piecewise closed line $\Gamma_U \cup \Gamma_R \cup \Gamma_D \cup \Gamma_L$ and spans the physical region of interest. Let $\mathbf{n}$ denote the outward pointing unit normal on the boundary of Ω_d. For the acoustic waves to leave the domain without significant spurious reflections, the following radiation condition is applied [1, Chapter 7]:

$$\frac{1}{\bar{\rho}}\nabla x \cdot \mathbf{n} = -\frac{1}{\bar{\rho}\bar{c}}\frac{\partial x}{\partial t}, \qquad \forall t \in \mathbb{R}^+, \forall \mathbf{p} \in \Gamma_L, \Gamma_R. \tag{2}$$

The FE method is based on the following weak or integral formulation of problem (1), that can be obtained by multiplying (1a) by a generic space-dependent test function $\psi(\mathbf{p})$, integrating over Ω_d, and by enforcing the boundary constraints (1c) and the radiation condition (2):

$$\begin{aligned} &\frac{d^2}{dt^2}\int_{\Omega_d}\frac{\psi x}{\bar{\rho}\bar{c}^2}\,d\mathbf{p} + \int_{\Omega_d}\frac{\nabla\psi\cdot\nabla x}{\bar{\rho}}d\mathbf{p} - \int_{\Omega_d}\frac{\psi f}{\bar{\rho}}\,d\mathbf{p} \\ &- \int_{\Gamma_U}\frac{\psi\nabla x\cdot\mathbf{n}}{\bar{\rho}}\,d\mathbf{p} + \frac{1}{\bar{\rho}\bar{c}}\bigg|_{\Gamma_L}\frac{d}{dt}\int_{\Gamma_L}\psi x\,d\mathbf{p} \\ &+ \frac{1}{\bar{\rho}\bar{c}}\bigg|_{\Gamma_R}\frac{d}{dt}\int_{\Gamma_R}\psi x\,d\mathbf{p} = 0. \end{aligned} \tag{3}$$

In the FE method, the pressure field $x(\mathbf{p}, t)$ is approximated by a linear combination of N_V known spatially-varying basis functions $\Phi_j(\mathbf{p})$, $j = 1, \ldots, N_V$,

$$x(\mathbf{p}, t) \simeq \sum_{j=1}^{N_V}\Phi_j(\mathbf{p})x_j(t) = \mathbf{\Phi}^T(\mathbf{p})\mathbf{x}(t), \tag{4}$$

where $x_j(t)$ is the j-th unknown expansion coefficient, and $\mathbf{\Phi}(\mathbf{p}) \in \mathbb{R}^{N_V}$ and $\mathbf{x}(t) \in \mathbb{R}^{N_V}$ are the column vectors

$$\mathbf{\Phi}(\mathbf{p}) \triangleq \mathrm{col}\{\Phi_j(\mathbf{p})\}_{j=1}^{N_V}, \quad \mathbf{x}(t) \triangleq \mathrm{col}\{x_j(t)\}_{j=1}^{N_V}. \tag{5}$$

The choice of the basis functions is a key issue of the FE algorithm and is directly linked to the type of elements. In the present implementation, the computational frame Ω_d is divided into a set of N_E non-overlapping triangles $\Omega_d = \bigcup_{e=1}^{N_E}\Omega_e, e = 1, \ldots, N_E$. This tessellation defines a mesh with N_V vertices $\mathbf{p}_j \in \Omega_d$, $j = 1, \ldots, N_V$, and each basis function $\Phi_j(\mathbf{p})$ is defined as a piecewise polynomial of first degree vanishing outside the elements around $\mathbf{p}_j$ and such that $\Phi_j(\mathbf{p}_i) = \delta_{ij}$, where δ_{ij} is the Kronecker delta. As a result, the j-th expansion coefficient $x_j(t)$ corresponds to the value of the approximation of the pressure field at the vertex $\mathbf{p}_j$.

To compute the N_V unknowns x_j, $j = 1, \ldots, N_V$, expansion (4) is first introduced in the weak form (3). Then, by replacing the generic test function ψ with the basis functions, we obtain the following system of N_V ordinary differential equations of second order in time:

$$\mathbf{M}\frac{d^2\mathbf{x}}{dt^2} + \mathbf{D}\frac{d\mathbf{x}}{dt} + \mathbf{K}\mathbf{x} - \mathbf{f} = 0, \tag{6}$$

where

$$\begin{aligned} \mathbf{M} &\triangleq \int_{\Omega_d}\frac{\mathbf{\Phi}(\mathbf{p})\mathbf{\Phi}^T(\mathbf{p})}{\bar{\rho}(\mathbf{p})\bar{c}^2(\mathbf{p})}d\mathbf{p}, \\ \mathbf{D} &\triangleq \frac{1}{\bar{\rho}\bar{c}}\bigg|_{\mathbf{p}\in\Gamma_L}\int_{\Gamma_L}\mathbf{\Phi}(\mathbf{p})\mathbf{\Phi}^T(\mathbf{p})\,d\mathbf{p} \\ &\quad + \frac{1}{\bar{\rho}\bar{c}}\bigg|_{\mathbf{p}\in\Gamma_R}\int_{\Gamma_R}\mathbf{\Phi}(\mathbf{p})\mathbf{\Phi}^T(\mathbf{p})\,d\mathbf{p}, \\ \mathbf{K} &\triangleq \int_{\Omega_d}\frac{\nabla\mathbf{\Phi}(\mathbf{p})\cdot\nabla\mathbf{\Phi}^T(\mathbf{p})}{\bar{\rho}(\mathbf{p})}d\mathbf{p}, \\ \mathbf{f}(t) &\triangleq s(t)\int_{\Omega_d}\frac{\mathbf{\Phi}(\mathbf{p})\delta(\mathbf{p}-\mathbf{p}^0(t))}{\bar{\rho}(\mathbf{p})}d\mathbf{p} = \frac{s(t)\mathbf{\Phi}(\mathbf{p}^0(t))}{\bar{\rho}(\mathbf{p}^0(t))} \end{aligned} \tag{7}$$

with *mass* matrix $\mathbf{M} \in \mathbb{R}^{N_V\times N_V}$, *damping* matrix $\mathbf{D} \in \mathbb{R}^{N_V\times N_V}$, *stiffness* matrix $\mathbf{K} \in \mathbb{R}^{N_V\times N_V}$, and forcing term

$\mathbf{f}(t) \in \mathbb{R}^{N_V}$. Then, by regularly discretizing in time (6) with sampling interval Δt such that $t_k = k\Delta t$, $k \in \mathbb{N}_0$, and by computing the approximations $\mathbf{x}_{k+1}$ and $\dot{\mathbf{x}}_{k+1}$ of $\mathbf{x}$ and its derivative $d\mathbf{x}/dt$ at time instant t_{k+1} through the Newmark's method [1], the following discrete-time linear state-space model is obtained:

$$\mathbf{z}_{k+1} = \mathbf{A}\,\mathbf{z}_k + \mathbf{B}\,\mathbf{u}_k + \mathbf{w}_k \tag{8}$$

where $\mathbf{z}_k \triangleq [\mathbf{x}_k^T\ \dot{\mathbf{x}}_k^T]^T$, $\mathbf{u}_k \triangleq [\mathbf{f}_k^T\ \mathbf{f}_{k+1}^T]^T$, $\mathbf{f}_k = \mathbf{f}(t_k)$, while the state transition matrix $\mathbf{A} \in \mathbb{R}^{2N_V \times 2N_V}$ and, respectively, the input matrix $\mathbf{B} \in \mathbb{R}^{2N_V \times 2N_V}$ are defined as follows

$$\mathbf{A} = \mathbf{G}\begin{bmatrix} \mathbf{I} - \frac{\Delta t^2}{2}(1-2\beta)\mathbf{M}^{-1}\mathbf{K} & \Delta t\mathbf{I} - \frac{\Delta t^2}{2}(1-2\beta)\mathbf{M}^{-1}\mathbf{D} \\ -\Delta t(1-\gamma)\mathbf{M}^{-1}\mathbf{K} & \mathbf{I} - \Delta t(1-\gamma)\mathbf{M}^{-1}\mathbf{D} \end{bmatrix},$$

$$\mathbf{B} = \mathbf{G}\begin{bmatrix} \Delta t^2\beta\mathbf{M}^{-1} & \frac{\Delta t^2}{2}(1-2\beta)\mathbf{M}^{-1} \\ \Delta t\gamma\mathbf{M}^{-1} & \Delta t(1-\gamma)\mathbf{M}^{-1} \end{bmatrix},$$

$$\mathbf{G} = \begin{bmatrix} \mathbf{I} + \Delta t^2\beta\mathbf{M}^{-1}\mathbf{K} & \Delta t^2\beta\mathbf{M}^{-1}\mathbf{D} \\ \Delta t\gamma\mathbf{M}^{-1}\mathbf{K} & \mathbf{I} + \Delta t\gamma\mathbf{M}^{-1}\mathbf{D} \end{bmatrix}^{-1},$$

where β and γ are non-negative parameters that determine the numerical accuracy and the stability properties of the time integration scheme, which is second-order accurate and unconditionally stable for $\beta = \gamma = 0.5$ [1]. Finally, note that $\mathbf{w}_k$ in (8) is a process disturbance modeling also approximation errors that originate from the above space-time discretization.

IV. Dynamic Source Localization

Based on the FE model of underwater acoustic propagation presented in Section III, we developed a source localization system that sequentially i) predicts the acoustic pressure field through the finite-dimensional approximation of the full wave equation; ii) assimilates the available observations collected by an array of acoustic sensors to correct the estimates of the acoustic field; iii) runs detection and localization strategies to recursively detect and estimate the position of a mobile acoustic source from the estimated source-induced field.

A. Multiple model approach

The key idea is to incorporate the source detection and localization processes into a *Multiple Model* (MM) tracking approach [3] to field estimation that assumes the evolution of system (8), at each time step, obeys to one of a finite set of possible modes of operation or propagation models. This makes it possible to match each hypothesis of the source being located in a generic element of the mesh to a distinct operating mode of the acoustic system, plus a null hypothesis accounting for the absence of the source in the monitored area.

System (8) for each mode $j = 1, 2, ..., N_E$ is then governed by the following mode-matched model associated to the hypothesis that a dynamic source is located in element Ω_j:

$$\begin{aligned} \mathbf{z}_{k+1} &= \mathbf{A}\mathbf{z}_k + \mathbf{B}_j\boldsymbol{\varphi}_k + \mathbf{w}_k \\ \mathbf{y}_k &= \mathbf{C}\,\mathbf{z}_k + \mathbf{v}_k \end{aligned} \tag{9}$$

where $\mathbf{y}_k$ is the vector of all measurements collected from an array of S sensors with noise vector $\mathbf{v}_k$ independent of $\mathbf{z}_k$ and representing the effect of undesired signals (e.g., ambient or thermal noise), $\boldsymbol{\varphi}_k$ contains the $2(d+1)$-dimensional column vector of stacked coefficients $\boldsymbol{\Phi}_\ell^j(\mathbf{p}_k^0)$, $\ell \in \mathcal{V}_j$, d being the dimension of the spatial domain, while $\mathbf{B}_j \in \mathbb{R}^{2N_V \times 2(d+1)}$ properly selects the columns of $\mathbf{B}$ corresponding to the nodes of element Ω_j, such that $\mathbf{B}\mathbf{u}_k = \mathbf{B}_j\boldsymbol{\varphi}_k$. It is worth noting that in order to be able to detect new sources, an extra *source-free* operating mode $j = 0$, based on the assumption that no point source is present, needs to be added to the set of $N_E + 1$ possible modes of the MM algorithm. The joint source position and field estimation is carried out by constructing an augmented system, as the aggregate of the original system (9) and a suitable model for the time evolution of the unknown input $\boldsymbol{\varphi}_k$, which takes the following form for $j = 1, 2, ..., N_E$

$$\begin{aligned} \begin{bmatrix} \mathbf{z}_{k+1} \\ \boldsymbol{\varphi}_{k+1} \end{bmatrix} &= \begin{bmatrix} \mathbf{A} & \mathbf{B}_j \\ \mathbf{0} & \mathbf{I} \end{bmatrix}\begin{bmatrix} \mathbf{z}_k \\ \boldsymbol{\varphi}_k \end{bmatrix} + \begin{bmatrix} \mathbf{w}_k \\ \boldsymbol{\varsigma}_k \end{bmatrix} \\ \mathbf{y}_k &= [\mathbf{C}\quad \mathbf{0}]\begin{bmatrix} \mathbf{z}_k \\ \boldsymbol{\varphi}_k \end{bmatrix} + \mathbf{v}_k \end{aligned} \tag{10}$$

whereas, for $j = 0$

$$\mathbf{z}_{k+1} = \mathbf{A}\mathbf{z}_k + \mathbf{w}_k, \qquad \mathbf{y}_k = \mathbf{C}\,\mathbf{z}_k + \mathbf{v}_k. \tag{11}$$

Note that in (10) the dynamics of the source-induced forcing terms in $\boldsymbol{\varphi}_k$ are assumed to vary slowly with time and, hence, to follow a discrete-time random walk. Given that the source may move within the domain, i.e. the correct operating mode may switch over time, it is convenient to employ the *Interacting Multiple Model* (IMM) [3], which allows for mode jumps, limiting at the same time the number of hypotheses to the number of filters.

B. Finite-element multiple model ensemble Kalman filter

For dynamic source localization, we run an IMM estimator for the system (10) with mode-to-mode transitions modelled by means of a homogeneous Markov chain with known transition probabilities

$$\pi_{ij} = \text{prob}\,(\nu_k = j \,|\, \nu_{k-1} = i)\,, \qquad i, j \in \{0, 1, ..., N_E\} \tag{12}$$

where ν_k is the *modal state* (i.e. the mode in operation) at time k. At the beginning of each sampling interval, the $N_E + 1$ filters interact in a mixing step which produces the mixed initial conditions for field estimation. The recursion of the proposed FE-MM-EnKF can be summarized as follows.

1. ***Mixing probability update:*** in order to calculate the mixed initial conditions, the mixing probabilities are first updated as follows

$$\mu_{k-1|k-1}^{j|i} \triangleq \pi_{ij}\,\mu_{k-1}^i \Big/ \sum_{\ell=0}^{N_E} \pi_{\ell j}\,\mu_{k-1}^\ell \tag{13}$$

2. ***Mixing:*** the mixed field estimates and covariances are computed as

$$\hat{\mathbf{z}}^{0j}_{k-1|k-1} = \sum_{i=0}^{N_E} \hat{\mathbf{z}}^{i}_{k-1|k-1} \mu^{i|j}_{k-1|k-1}$$

$$\mathbf{P}^{0j}_{k-1|k-1} = \sum_{i=0}^{N_E} \mu^{j|i}_{k-1|k-1} \left[\mathbf{P}^{i}_{k-1|k-1} + \tilde{\mathbf{z}}^{ij} (\tilde{\mathbf{z}}^{ij})^T \right] \quad (14)$$

where $\hat{\mathbf{z}}^{i}_{k-1|k-1}$ and $\mathbf{P}^{i}_{k-1|k-1}$ denote respectively the mode-conditioned field estimates and covariances at time step $k-1$. Note that $\tilde{\mathbf{z}}^{ij}$ in (14) is the spread of the means defined in [3] as $\tilde{\mathbf{z}}^{ij} = \hat{\mathbf{z}}^{i}_{k-1|k-1} - \hat{\mathbf{z}}^{0j}_{k-1|k-1}$.

3. ***Mode-matched ensemble Kalman filtering:*** each mode-matched filter carries out the prediction and correction steps, processing the entire vector $\mathbf{y}_k$ of gathered measurements. The parallel mode-matched filters are implemented in the EnKF fashion for computationally efficient field estimation that implies large-scale processing of the finite-element system. The bank of EnKFs produces an ensemble of q augmented state estimates $\hat{\boldsymbol{\chi}}^{j}_{k|k} \triangleq [\hat{\mathbf{z}}^{j^T}_{k|k} \, \hat{\boldsymbol{\varphi}}^{j^T}_{k|k}]^T$ with sample error covariance $\boldsymbol{\mathcal{P}}^{j}_{k|k}$ for each mode $j \in \{0, 1, \ldots, N_E\}$, q being the ensemble size. In addition, assuming Gaussian noises, the mode likelihoods are evaluated as

$$\Lambda^{j}_{k} = \mathcal{N}(\boldsymbol{\zeta}^{j}_{k}; \mathbf{0}, \mathbf{S}^{j}_{k}), \quad j = 0, 1, \ldots, N_E \quad (15)$$

where $\boldsymbol{\zeta}^{j}_{k} \triangleq \mathbf{y}_k - \mathbf{C}\hat{\mathbf{z}}^{j}_{k|k-1}$ is the innovation at time k of mode j, and $\mathbf{S}^{j}_{k}$ the associated covariance.

4. ***Mode probability update:*** assuming that mode transitions are modeled by (12), the mode probabilities are computed as follows

$$\mu^{j}_{k} = \frac{1}{c_1} \Lambda^{j}_{k} \sum_{i=0}^{N_E} \pi_{ij} \, \mu^{i}_{k-1} \quad (16)$$

where $c_1 = \sum_{j=0}^{N_E} \Lambda^{j}_{k} \sum_{i=0}^{N_E} \pi_{ij} \, \mu^{i}_{k-1}$ is the normalization constant.

5. ***Source localization:*** At the end of each cycle, the mode j^* with highest probability, i.e. $j^* = \arg\max_j \mu^{j}_{k}$ is considered as the operating one and the associated mode-conditioned estimate is directly used for field estimation. Then, exploiting the structure of the FE approximation, the source location can be estimated as a convex combination of the position of the vertices of Ω_{j^*} matched to the estimated operating mode, i.e. $\hat{\mathbf{p}}^{0}_{k} = \sum_{i \in \mathcal{V}_{j^*}} \hat{\varphi}^{i}_{k} \, \mathbf{p}_i$, where $\hat{\varphi}^{i}_{k}$ denotes the entry of $\hat{\boldsymbol{\varphi}}^{j^*}_{k|k}$ corresponding to vertex i of Ω_{j^*}.

Note that the computational complexity of the proposed FE-MM-EnKF mainly involves the number of nodes N_V with $2N_V$ as the dimension of the acoustic field, the ensemble size q, the number of finite elements N_E corresponding to $N_E + 1$ mode-matched EnKFs, and the number of sensors S. In particular, the complexity of a single mode-matched EnKF is $\mathcal{O}(nqS)$, where $n = 2(N_V + d + 1)$, computationally cheaper than standard Kalman filters if n is very large and $q \ll n$, while the mixing steps of the IMM implementation yield $N_E + 1$ hypotheses with $N_E + 1$ mode-matched filters.

V. Simulation results

We simulated a moving source transmitting a signal of frequency $f_0 = 30$ Hz for $K = 500$ time steps (with time integration step $\Delta t = 0.01$ s) in a shallow water environment with an isospeed water column ($c = 1500$ m/s, $\rho = 1000$ kg/m^3) of 25 m depth and 150 m long. The acoustic pressure field generated by the dynamic source is measured, with sampling interval $T_s = 0.01$ s, using a uniform rectangular array of acoustic sensors (see Fig. 2). For each simulation, we set the following filter parameters: initial guess of acoustic pressure $\hat{x}_{1|0} = 0.01$ Pa all over the domain, standard deviation of measurement noise $\sigma_v = 0.1$ μPa, standard deviation of process noise $\sigma_w = 0.08$ μPa, and ensemble size $q = 50$. The mixing probabilities were initialized as uniformly distributed. The transition probabilities in (12) were chosen as $\pi_{ii} = 0.99$, $\forall i = 0, 1, \ldots, N_E$, with 0.008 and 0.002 probability equally assigned to all adjacent and, respectively, non-adjacent elements to the current modal state. To evaluate the performance of the proposed filter, we considered the following parameters: number of sensors $S = 30$, mesh size ratio MSR $= 0.8$, which represents the accuracy of the finite-element underwater acoustic model used by the filter with respect to the ground truth, and different levels of signal-to-noise ratio. The MSR is defined as MSR $\triangleq L_f / L_g$ where L_f and L_g are the mean element size of the finite-element mesh used by, respectively, the filter and the ground truth simulator. Given the standard deviation of noise σ_y at each sensor of the array, the SNR can be defined as [1, Chapter 10] SNR $\triangleq 10 \log_{10}(\sum_{k=1}^{K} \text{SNR}_k / K)$ where $\text{SNR}_k \triangleq \frac{1}{S} \sum_{i=1}^{S} x^2_{k,i} / \sigma^2_y$ is the SNR at time k, and $x_{k,i}$ is the acoustic pressure on the i-th sensor at time k.

In Fig. 2 we show an example of the actual trajectory of the source compared to the estimated positions obtained by applying the proposed FE-MM-EnKF with MSR $= 0.8$, SNR $=$ 10 dB, and $S = 30$. We can see the computational domain, the FE mesh ($N_V = 97$, $N_E = 150$, $L_f = 8.75$ m), the uniform rectangular array of sensors, and the source moving with constant velocity for K time steps and covering 25 m in range at a speed of 5 m/s. We note that, even if the initial (first four) estimates are far from the real trajectory, the estimated trajectory converges to the actual one as soon as the source is correctly detected and tracked in the exact element of the mesh (see the performance in terms of mode estimation and mean absolute error shown respectively in Fig. 3(a) and Fig. 3(b)). In Fig. 3(a) we show the mode estimation performance where we can see in particular that the source is detected at each time step as the estimated mode is such that $j^* \neq 0$. Furthermore, we can accurately predict the element of the mesh where the source is located, although there are slight delays due to mode-to-mode transitions. In Fig. 3(b) we show the mean absolute error of the estimated source position over time, which, after the initial estimates, remains below 1 m for the entire simulation. Finally, in Fig. 4 we show the performance of the FE-MM-EnKF in terms of the time-averaged root mean square error of the estimated source position (RMSE$_{pos}$) over four different levels of SNR. The RMSE in position is defined

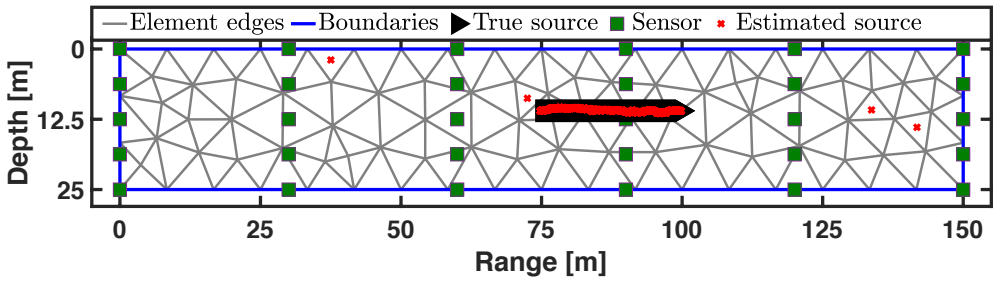

Fig. 2: Simulated environment with MSR $= 0.8$, SNR $= 10$ dB, and $S = 30$: estimated source positions vs ground truth.

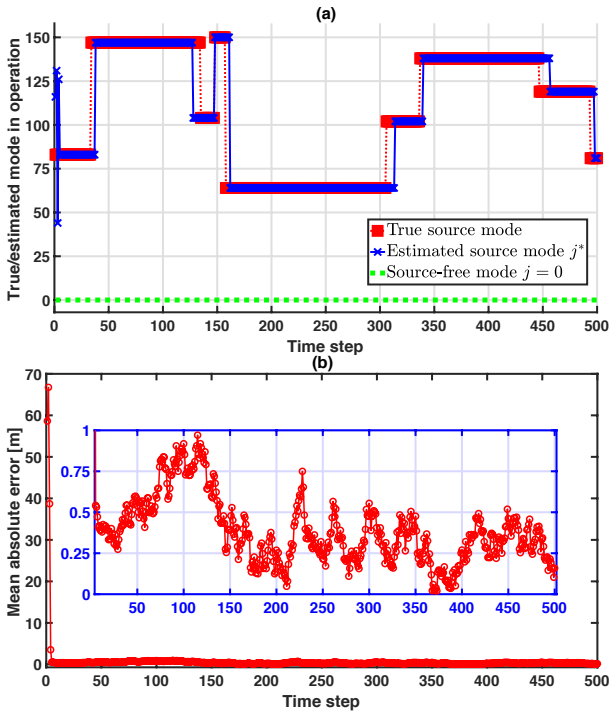

Fig. 3: (a) Source mode estimation over time, and (b) mean absolute error of the estimated source position over time with MSR $= 0.8$, SNR $= 10$ dB, and $S = 30$.

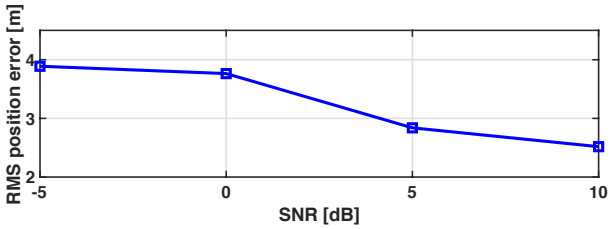

Fig. 4: RMSE$_{pos}$ vs SNR with MSR $= 0.8$ and $S = 30$.

as $\text{RMSE}_{pos} \triangleq \sum_{k=1}^{K} \text{RMSE}_{pos,k}/K$, where $\text{RMSE}_{pos,k} \triangleq \sqrt{\sum_{j=1}^{M} (\hat{\mathbf{p}}_{k,j}^0 - \mathbf{p}_{k,j}^0)^2/M}$ is the error at time k, $\hat{\mathbf{p}}_{k,j}^0$ and $\mathbf{p}_{k,j}^0$ denote the estimated and, respectively, true source position in the j-th Monte Carlo run, and $M = 100$ is the total number of runs. The localization performance is strong at all levels of SNR, with the error decreasing as the SNR increases.

VI. Conclusions

This paper focused on the development of a novel multiple-model approach to source detection and dynamic localization based on a finite-element model of underwater acoustic propagation and measurements from acoustic sensors. Simulation experiments demonstrated the capability of the proposed FE-MM-EnKF in noisy environments. Future work will explore the application to real-world underwater complex environments, and the extension to underwater multi-target tracking.

References

[1] F. B. Jensen, W. A. Kuperman, M. B. Porter, and H. Schmidt, *Computational Ocean Acoustics*. New York, NY: Springer New York, 2011.

[2] A. B. Baggeroer, W. A. Kuperman, and P. N. Mikhalevsky, "An overview of matched field methods in ocean acoustics," *IEEE Journal of Oceanic Engineering*, vol. 18, no. 4, pp. 401–424, 1993.

[3] Y. Bar-Shalom, X. R. Li, and T. Kirubarajan, *Estimation with applications to tracking and navigation*. John Wiley & Sons, 2001.

[4] A. Farina, "Target tracking with bearings-only measurements," *Signal Processing*, vol. 78, no. 1, pp. 61–78, 1999.

[5] P. Braca, P. Willett, K. LePage, S. Marano, and V. Matta, "Bayesian tracking in underwater wireless sensor networks with port-starboard ambiguity," *IEEE Transactions on Signal Processing*, vol. 62, no. 7, pp. 1864–1878, 2014.

[6] A. Tolstoy, "Sensitivity of matched field processing to sound-speed profile mismatch for vertical arrays in a deep water Pacific environment," *J. Acoust. Soc. Am.*, vol. 85, no. 6, pp. 2394–2404, 1989.

[7] C. A. Zala and J. M. Ozard, "Matched-field processing for a moving source," *The Journal of the Acoustical Society of America*, vol. 92, no. 1, pp. 403–417, 1992.

[8] S. Tantum, L. Nolte, J. Krolik, and K. Harmanci, "The performance of matched-field track-before-detect methods using shallow-water Pacific data," *J. Acoust. Soc. Am.*, vol. 112, no. 1, pp. 119–127, 2002.

[9] S. E. Dosso and M. J. Wilmut, "Bayesian acoustic source track prediction in an uncertain ocean environment," *IEEE Journal of Oceanic Engineering*, vol. 35, no. 4, pp. 811–820, 2010.

[10] A. Gunes and M. B. Guldogan, "Joint underwater target detection and tracking with the Bernoulli filter using an acoustic vector sensor," *Digital Signal Processing*, vol. 48, pp. 246–258, 2016.

[11] K. Nagananda and G. Anand, "Underwater target tracking with vector sensor array using acoustic field measurements," in *OCEANS 2017*.

[12] W. Yi, L. Fu, A. F. Garcia-Fernandez, L. Xu, and L. Kong, "Particle filtering based track-before-detect method for passive array sonar systems," *Signal Processing*, vol. 165, pp. 303–314, 2019.

[13] R. Sabatini, O. Marsden, C. Bailly, and O. Gainville, "Three-dimensional direct numerical simulation of infrasound propagation in the Earth's atmosphere," *Journal of Fluid Mechanics*, vol. 859, p. 754–789, 2019.

[14] G. Battistelli, L. Chisci, N. Forti, G. Pelosi, and S. Selleri, "Point source estimation via finite element multiple-model Kalman filtering," in *54th IEEE Conference on Decision and Control*, pp. 4984–4989, 2015.

[15] G. Battistelli, L. Chisci, N. Forti, G. Pelosi, and S. Selleri, "Distributed finite-element Kalman filter for field estimation," *IEEE Transactions on Automatic Control*, vol. 62, no. 7, pp. 3309–3322, 2017.

[16] G. Evensen, *Data assimilation: the ensemble Kalman filter*. Springer Science & Business Media, 2009.